Wideband MIMO channel sounder for radio measurements in the 60 GHz band

S. Salous, *SMIEEE,* S.M. Feeney, X. Raimundo and A.A. Cheema

***Abstract*— Applications of the unlicensed 60 GHz band include indoor wireless local area networks, outdoor short range communications and on body networks. To characterise the radio channel for such applications, a novel digital chirp sounder with programmable bandwidths up to 6 GHz with switched two transmit channels and two parallel receive channels for Multiple Input Multiple Output (MIMO) measurements was realised. For waveform durations of 819.2 μs, Doppler measurements can be performed up to 610 Hz for the single transmit and two receive configuration or 305 Hz for MIMO measurements. In this paper we present the architecture of the sounder and demonstrate its performance from back to back tests and from measurements of *rms* delay spread, path loss and MIMO capacity in an indoor and an outdoor environment. For 20 dB threshold, the rms delay spread for 90% of the measured locations is estimated at 1.4 ns and 1 ns for the indoor and outdoor environments, respectively. MIMO capacity close to the iid channel capacity for 2 by 2 configuration is achieved in both environments.**

***Index Terms*— Chirp, FMCW, frequency sweep, MIMO, mm wave, path loss, PRBS, propagation, *rms* delay spread, sounder, 60 GHz.**

I. INTRODUCTION

THE 60 GHz band has attracted more interest in recent times due to the large available bandwidth with the ITU-R recommending four 2.16 GHz wide channels centred on 58.32 GHz, 60.48 GHz, 62.64 GHz and 64.80 GHz, thus enabling high data rates and video streaming. As it falls in the oxygen absorption band, the 60 GHz band also facilitates frequency reuse and covert communication such as for on-body networks for the dismounted soldier. In addition, the small wavelength enables the use of beamforming with multiple antennas to overcome the higher path loss. This prompted the development of IEEE802.15.3c standard for wireless personal area networks and the IEEE 802.11ad standard for wireless local area networks for data rates on the order of 6.75 Gbps using approximately 2 GHz of spectrum with single and multi-carrier schemes. To enable the evaluation of the 60 GHz radio channel a number of channel sounders and measurements have been reported. These include pseudo random binary sequences (PRBS) based sounders with varying clock rates from 100 MHz to 3.5 GHz with single or dual polarised antennas [1-7]. The frequency swept method with vector network analysers (VNA) has been used either with up and down converters [8-10] or more recently with 60 GHz VNA's [11]. The VNA provides a ready to use solution for short range and for on-body networks, but it suffers from a slow sweep rate which does not capture the time variability of the channel and has limited range due to the need to connect cables to the transmitter and to the receiver. While the loss due to the use of RF cables at 60 GHz can be compensated by the use of an additional amplifier, the non-linear phase of the cables over the swept bandwidth and the phase instability distort the measured channel response. Another approach is to use an optical fibre cable over the link to feed the reference signal to the receiver [12]. An alternative sounding waveform is the digital frequency sweep at both the transmitter and the receiver with various up converter stages and frequency multiplication [13].

In this paper we present the architecture and measurement results obtained with a compact channel sounder with 2 transmit channels switched at the waveform repetition rate and two parallel receive channels for both single antenna and multiple antenna measurements in the 60 GHz band. This paper is organised as follows: in section II we discuss the overall design concept and compare the possible architectures of channel sounders. Section III gives details of the realised sounder blocks and their performance, and section IV describes the overall performance with back to back tests. We also present results of *rms* delay spread from measurements performed in an indoor and an outdoor environment, path loss coefficient and MIMO capacity gains.

II. DESIGN CONCEPT OF THE DIGITAL SWEEP SOUNDER

The requirements of a versatile channel sounder in the millimeter wave band with multiple switched transmit antennas for various measurements including on-body networks dictate that the transmitter and receiver units are portable and that switching and RF cable phase instability at 60 GHz are avoided. Other requirements are the time delay resolution, the maximum Doppler shift, and the sampling rate for data acquisition. For high data rate applications and on-body measurements, the desired spatial resolution is on the

Manuscript received October, 27, 2014,; revised June, 2, 2015, November 12, 2015 and December, 1st, 2015; accepted December 1st, 2015. This work was supported by EPSRC EP/I00923X/1 PATRICIAN project, and EPSRC Impact Acceleration Account. A. Cheema and X. Raimundo studentships were funded by the School of Engineering and Computing Sciences at Durham University.

The authors are with the School of Engineering and Computing Sciences, Durham University, Durham, UK, DH1 3LE. (e-mail: sana.Salous@ durham .ac.uk)

order of 5-15 cm which corresponds to 2-6 GHz bandwidth. One method to generate the required high bandwidth is to concatenate ten 500 MHz frequency sections as in [3].

The majority of the reported sounders in the 60 GHz band use the PRBS technique with clock rates ranging from 100 MHz [6] to 3.5 GHz [7] and use either a sliding correlator to achieve bandwidth compression as in [7] or a high speed digitising scope as in [3]. An alternative is to use a digital frequency sweep generated using a direct digital frequency synthesiser (DDFS) as in [12-13]. Thus far, the highest reported resolution is 1 ns [5, 7]. In this paper we present a two by two MIMO sounder with direct down conversion to baseband with a high programmable bandwidth up to 6 GHz and high repetition rate. In this section we briefly outline the chirp sounding technique followed by detailed description of the sounder.

A. Overview of frequency swept sounding

A frequency swept signal is represented by a linear decrease or increase of the instantaneous frequency f_i over a bandwidth B Hz in T seconds as in (1) where the sweep rate k is equal to B/T, f_c is the carrier frequency and the plus sign indicates a frequency increase.

$$f_i = f_c + \frac{B}{T}t = f_c + kt \qquad -\frac{T}{2} < t < \frac{T}{2} \tag{1}$$

This gives a linearly frequency modulated signal as in (2).

$$s(t) = \cos(\omega_c t + \pi k t^2) \qquad -\frac{T}{2} < t < \frac{T}{2} \tag{2}$$

where $\omega_c = 2\pi f_c$

The received signal consists of the sum of amplitude scaled and time delayed replicas representing the multipath components as in (3).

$$s_R(t) = \sum_{i=1}^{N} \mathrm{A}_i \cos(\omega_c(t - t_i) + \pi k(t - t_i)^2) \tag{3}$$

where A_i and t_i are the amplitude and time delay of the i^{th} multipath component, respectively and N is the total number of multipath components.

The received signal is mixed with a locally generated replica as in (4).

$$s(t).s_R(t) = cos(\omega_c t + \pi k t^2).\sum_{i=1}^{N} A_i \cos(\omega_c(t - t_i) + \pi k(t - t_i)^2) \tag{4}$$

This results in the sum and difference frequencies which when low pass filtered gives the difference frequency as in (5.a). This simplifies to the expression in (5.b) which can be rewritten in a more compact form as in (5.c).

$$\big(s(t).s_R(t)\big)_{LPF} = \sum_{i=1}^{N} \mathrm{B}_i \cos\big(\omega_c(t - t_i) + \pi k(t - t_i)^2 - (\omega_c t + \pi k t^2)\big) \tag{5.a}$$

$$\big(s(t).s_R(t)\big)_{LPF} = \sum_{i=1}^{N} \mathrm{B}_i \cos(2\pi k t t_i + \omega_c t_i - \pi k t_i^2) \tag{5.b}$$

$$\big(s(t).s_R(t)\big)_{LPF} = \sum_{i=1}^{N} \mathrm{B}_i \cos(2\pi k t t_i + \varphi_i) \tag{5.c}$$

where B_i is the detected amplitude of the i^{th} multipath component taking into account the overall gain in the receiver, and $\varphi_i = \omega_c t_i - \pi k t_i^2$.

This gives the sum of N beat notes where the beat note for the i^{th} multi-path component has a frequency f_{iR} equal to kt_i as in (6).

$$(f_{iR})_{LPF} = kt_i \tag{6}$$

Thus spectrum analysis of the filtered output delineates the multipath components. Equation (6) indicates that the received signal has a baseband frequency range related to the maximum time delay between the transmitter and the receiver frequency sweeps or equivalently to the time delay of the farthest multipath component and the sweep rate. Thus the technique enables bandwidth compression at the receiver which facilitates the sounding with the desired 6 GHz bandwidth for fine time delay resolution. The Waveform Repetition Frequency (*WRF=1/T*) or equivalently the duration of the sweep T is normally chosen to be significantly longer than the maximum expected time delay but sufficiently short to cover the maximum Doppler shift, f_{Dmax}=*WRF/2*.

The frequency sweep can be generated using analogue techniques with voltage controlled oscillators (VCO), digital techniques using DDFS in programmable steps or hybrid techniques with a DDFS driving a phase locked loop [14]. The DDFS generates the frequency in steps Δf Hz in Δt seconds, which is related to the clock rate of the synthesiser and the architecture of the phase accumulator. The effect of the discrete frequency steps is to generate unwanted components in the compressed output at a frequency equal to $(1/\Delta t)$ with an amplitude equal to $12.95 + 20\log(\frac{1}{\Delta f \Delta t})$ below the wanted signal [14]. The amplitude quantisation is determined by the number of bits in the digital to analogue converter (DAC). Current DDFS's can generate 1-1.25 GHz baseband bandwidths with 12 bit DAC clocked at rates up to 2.25 GHz. Higher bandwidths can be realised using the DDFS in conjunction with frequency multipliers which increases the sweep rate *k*, the frequency step size and the compressed bandwidth by the multiplication factor N. This gives an increase of the unwanted components by a factor of $20logN$.

SOUNDER DESIGN: The sounder consists of three main sub modules housed in a 3U 19 inch rack as shown in Fig. 1 (one at the transmitter and one at the receiver) and two portable units for the final up conversion to 60 GHz as shown in Fig. 2. The outputs of the receiver are digitised with a two channel 14 bit ADC card with a maximum sampling rate of 400 MHz per channel. The card enables the acquisition of continuous long records of data, and can be frequency locked to the rubidium frequency standard with a trigger input synchronised to the start of each frequency sweep for post-processing.

Main rack modules: One module contains the rubidium clock, a reference distribution board, UPS board and batteries

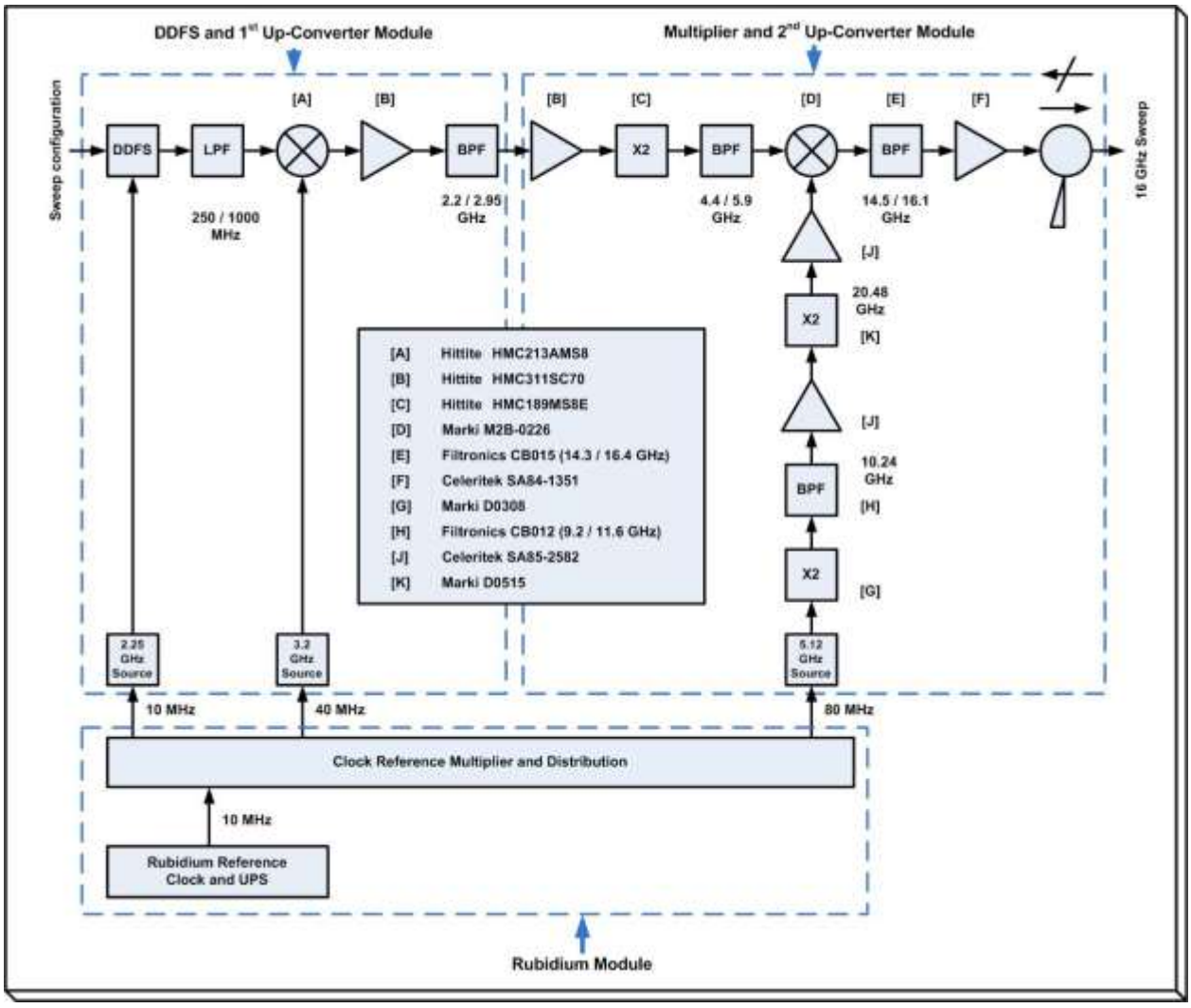

(a)

Rubidium standard and Reference distribution module

DDFS and first up converter module

Frequency multiplier and second up converter module

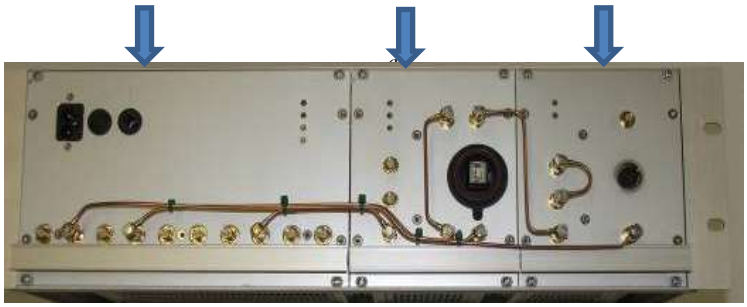

(b)

Fig. 1. Channel sounder sweep generator at various IF frequencies (a) block diagram, (b) realised units housed in 3U rack

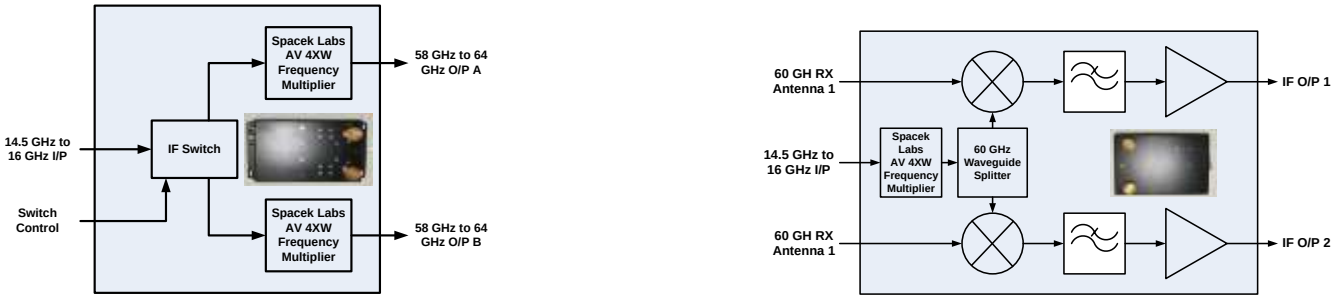

(a) (b)

Fig. 2. Block diagram of 60 GHz sounder (a) transmitter, (b) receiver

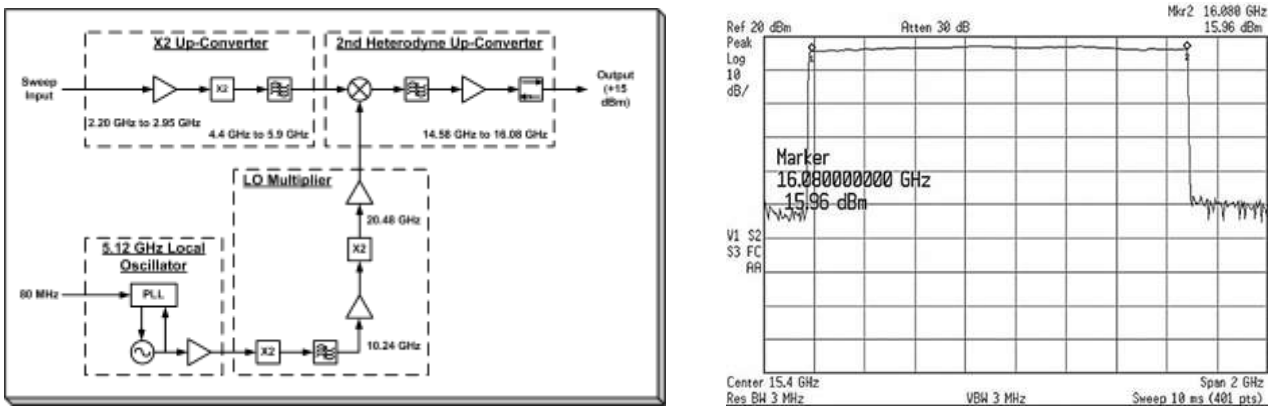

(a) (b)

Fig. 3. (a) Block diagram of up-converter to 16 GHz, (b) spectrum of sweep in the 14.5-16 GHz range

for keeping the rubidium warm in the event of disconnecting the unit from its power supply. The reference distribution takes the 10 MHz clock input from the Rubidium and generates several outputs at 10 MHz, 20 MHz, 40 MHz and 80 MHz to provide reference clocks to the various phase locked loops and clock for the analogue to digital converter in the data acquisition unit.

To enable multi-band channel measurements, in addition to the DDFS baseband output (dc-1 GHz), the other two modules generate three intermediate frequencies (IF) as illustrated in Fig. 1.a. The second module contains the DDFS and the first up-converter that covers the LTE band and one of the ISM bands (2.2-2.9 GHz). It has two custom designed phase locked loops (PLL) to generate the DDFS clock and a second PLL to generate the carrier for the up-converter at 3.2 GHz and two filters. The DDFS is a commercial board that implements a double accumulator, a sine look up table and has a 12-bit high speed DAC. Its frequency update rate is equal to the clock frequency divided by 32 which enables the generation of short duration sweeps or equivalently high waveform repetition rates for high Doppler coverage. The DDFS has the capability of either to free run or to be synchronised to an external trigger signal with programming via a USB interface. The DDFS also allows clearing the residual phase at the start of each sweep which gives phase coherence between sweeps for Doppler measurements.

The third module shown in Fig. 3.a has a Hittite (HMC189MS8E-2) frequency doubler to give an output from 4.4-5.9 GHz which covers the C band and the ISM band at 5.8 GHz. The multiplier output is bandpass filtered and then mixed using a Marki Microwave M2B-0226 mixer with a 20.48 GHz local oscillator (LO) to generate the IF at 14.5-16 GHz with a nominal level of ~16 dBm as shown in Fig. 3.b. The 20.48 GHz LO is implemented using a 5.12 GHz PLL with 80 MHz reference clock followed by two stages of frequency doublers. The first doubler from 5.12 GHz to 10.24 GHz uses a Marki Microwave D-0308, followed with a band pass filter (a Filtronic CB012 9.2 GHz to 12.6 GHz) and an amplifier (Celeritek SA85-2582). This is followed by a second doubler from 10.24 GHz to 20.48 GHz using a Marki Microwave D-0515 doubler and a second Celeritek SA85-2582 amplifier. The output is then fed to a circulator to provide the IF for the portable RF modules.

Portable 60 GHz MIMO modules: At the transmitter the 14.5-16 GHz signal is routed via low loss phase stable cables to two separate Spacek Labs AV-4XW X4 active frequency multiplier modules via a two way PIN switch which has more than 100 dB of channel isolation. Each transmitter channel provides an active power nominally +7 dBm (5 mW).

At the receiver, the 14.5-16 GHz signal is similarly multiplied by a Spacek Labs AV-4XW X4 active frequency multiplier followed by a 3 dB multi-hole directional coupler to form the LO for the down conversion mixers. The directivity of the directional coupler in addition to the LO/RF isolation provided a measured channel isolation of more than 50 dB.

The output of each receiver unit is pre-amplified with a 40

dB gain amplifier with ~5 dB noise figure, and the mixer conversion loss is ~7 dB. Including image noise the total receiver noise figure is ~15 dB.

A total multiplication factor of 8 from baseband gives a maximum of 6 GHz instantaneous bandwidth with 18 dB degradation in the level of the unwanted components. For the current DDFS, the switching speed is 14.88 ns, which gives an unwanted signal level of 71.45 dB below the wanted output for 4.4 GHz bandwidth with 819.2 μs sweep duration. This is comparable to the quantisation noise level of the 12 bit DAC in the DDFS board.

The PLL's use digital phase/frequency comparators which have a phase noise floor proportional to frequency. The phase noise degradation due to division within the PLL is proportional to the frequency squared [15]. Subject to the actual noise floor of the Rubidium's reference at 10 MHz and the noise performance of the PLL digital devices the net phase noise degradation can be minimised by exploiting multiplication of the reference. Here we have been able to exploit this technique at 3.2 GHz using a 40 MHz reference and at 5.12 GHz with 80 MHz reference to gain a net improvement in the phase noise of ~6 dB and ~8 dB respectively. The PLLs use relatively wide closed loop bandwidths (~100 kHz) with high phase margin (~75˚). This approach minimises "noise bumps" in the phase noise response and is highly tolerant to loop parameter changes.

Wideband performance of the sounder from back to back tests: The wideband performance of the sounder was verified from back to back tests to evaluate the isolation between the MIMO transmit and receive channels, overall phase noise, degradation due to the frequency multiplication, and overall dynamic range. The isolation between the channels and the phase noise was estimated by replacing the DDFS sources with signal generators to produce a constant continuous wave at the output of the receiver at 1 MHz. Fig. 4.a shows the measured isolation between the receive channels to be in excess of 50 dB. Similarly the output from the receiver channel when the transmitter output channels are switched was found to give ~100 dB of transmitter isolation which is consistent with the specifications of the switch. The total system signal to noise ratio due to phase noise is shown in Fig. 4.b to be ~52 dB at 300 Hz bandwidth.

To measure the overall dynamic range of the sounder, the transmitter output was connected to the receiver via a cascade of fixed programmable attenuators with 105 dB overall attenuation range. The sounder was programmed to generate a 4.4 GHz sweep in 819.2 μs. Fig. 5 displays the results for three levels of attenuation. With 105 dB attenuation between the transmitter and receiver, the signal level detected at the input of the receiver is ~-98 dBm, which corresponds to the output of the transmit power of 7dBm -105 dB attenuation. The signal to noise ratio (SNR) of the sounder for this attenuation level is seen to be in excess of 20 dB. Two other values of attenuation are shown in the figure corresponding to 95 dB and 85 dB with corresponding signal levels of -89 dBm and ~-80 dBm which are within the tolerance of the attenuator.

The compressed signal in Fig. 5 is seen to have sidebands

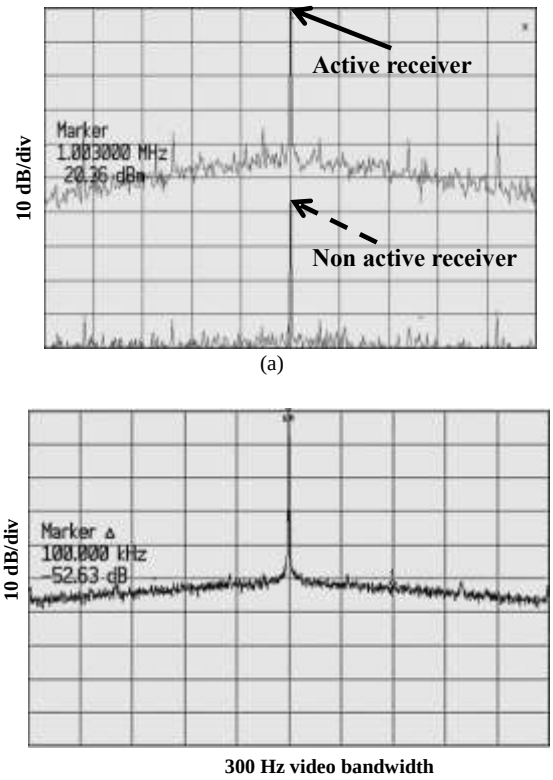

Fig. 4. Performance tests of the sounder (a) isolation between the receiver units, (b) overall phase noise in 300 Hz resolution bandwidth

due to the imperfections of the system's overall response. Compensation in the frequency domain using calibration files can significantly reduce the sidelobes. Fig. 6 illustrates that the compensated back to back response has a dynamic range in excess of 30 dB. The data were compensated using a back to back file of a different attenuation level and from a file obtained in close proximity over the air when the transmit and receive horn antennas used in the measurements were pointed at each other in an anechoic environment. Both calibration methods are seen to give similar results for the main lobe.

III. MIMO measurements

The sounder was used to collect data using horn antennas at the transmitter and at the receiver in an indoor environment and an outdoor environment. The antennas have a theoretical main lobe 3 dB width of 16.4^{o} in the H plane and 13.7^{o} in the E plane, a main lobe gain of 20.7 dBi and a first sidelobe level of -38.6 dB in the H plane and -18.2 dB in the E plane. The performance of the antenna and the coupling between antennas at the transmitter and receiver were measured using a 67 GHz Keysight VNA in the anechoic chamber at Durham University. The measured S11 and S12 parameters over the frequency range of interest are displayed in Fig. 7.a-b.

The S11 parameter is seen to be better than -10 dB which is consistent with the theoretical value of the antenna. The S12 parameter which estimates the coupling between antennas for the given separations and orientations at the transmitter (7 cm)

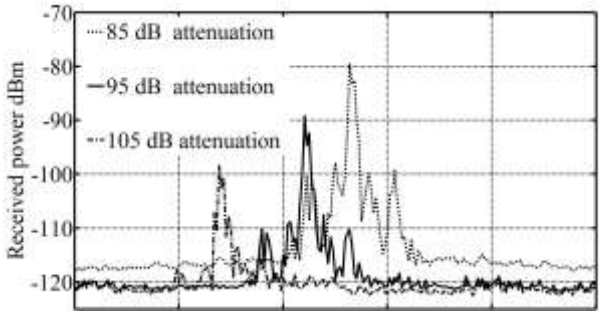

Fig. 5. Sensitivity and dynamic range test of the sounder in the 60 GHz band

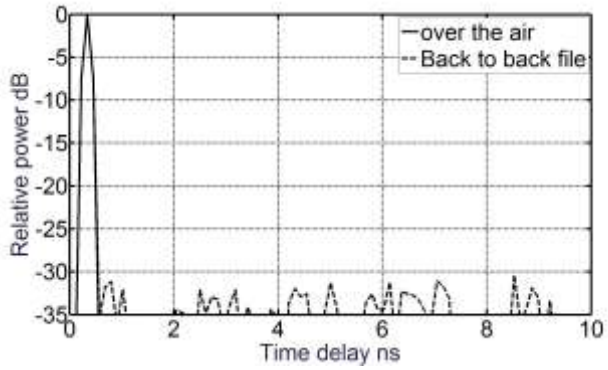

Fig. 6. Compensated response of the sounder from back to back tests and over the air test

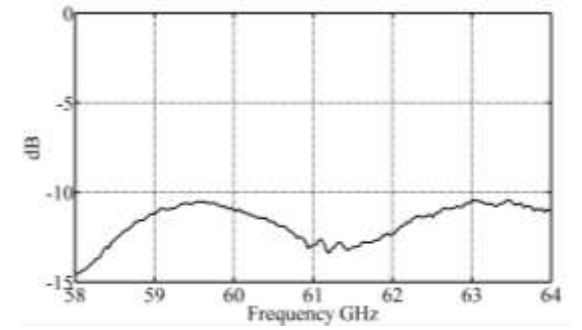

(a)

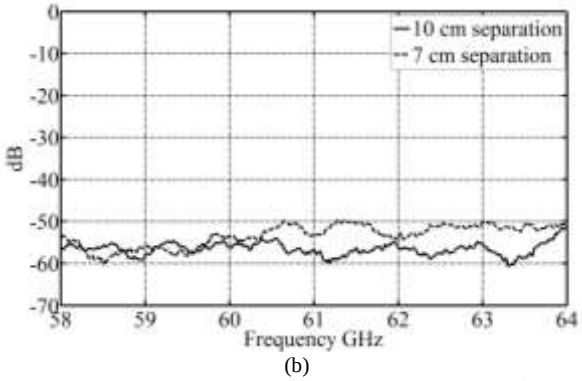

(b)

Fig. 7 (a) Measured S11 parameter, (b) Measured S12 parameter for antenna separation of 7 cm, and 10cm

and the receiver (10 cm) is seen to be below -50 dB indicating acceptable performance for MIMO measurements. The four antenna gains were also measured in the anechoic chamber with two antennas exhibiting a gain of 18 dBi and the other two antennas a gain of 19.6 dBi.

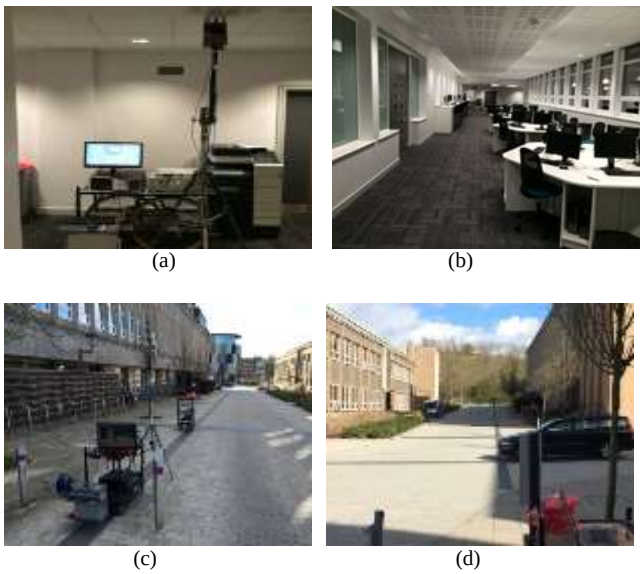

(a) (b) (c) (d)

Fig. 8 (a-b) Indoor measurement environment, (c-d) outdoor measurement environment

Fig. 8 shows the two measured environments where in the indoor environment the transmitter unit was raised to the ceiling level of about 2.35 m and the receiver antenna was mounted on the trolley at ~1.5 m. Similar antenna heights were used in the outdoor environment. The indoor environment is an L shaped room which extends up to ~38 m and has glass windows to one side with round tables, chairs and computers. The other side has partially glass façade as seen in Fig. 8.b. At the end of the room, a glass door and a window separate the room from the corridor. The outdoor environment has buildings on either side with 3-4 storeys, an open wider area with buildings to either side and a round shaped building with glass façade as seen in Fig. 8.c-d. During these measurements the receiving and transmitting antennas were pointed toward each other.

Fig. 9.a-b display the power delay profiles for one of the locations in the indoor environment and the outdoor environments respectively. The indoor environment is seen to exhibit significant multipath with a strong multipath component at about 100 ns indicating a 30 m reflection after the main component. Similarly Figs. 10 a-b display one of the MIMO channels versus distance for both the indoor and the outdoor environments.

The data were analysed to estimate the path loss by estimating the received power from the area under the power delay profile, the rms delay spread, the width of the power delay profile and the MIMO capacity. The data from the four channels were grouped into a single data pool to increase the data points in the estimation of the cumulative distribution. For the current set of data this resulted in 408 data points in the indoor environment and 292 for the outdoor environment. Fig. 11 displays the rms delay spread for 20 dB threshold for the two measured environments with summaries in Table I of the 50%, 90% and 95% values for both the width of the power delay profile and the rms delay spread. The results indicate

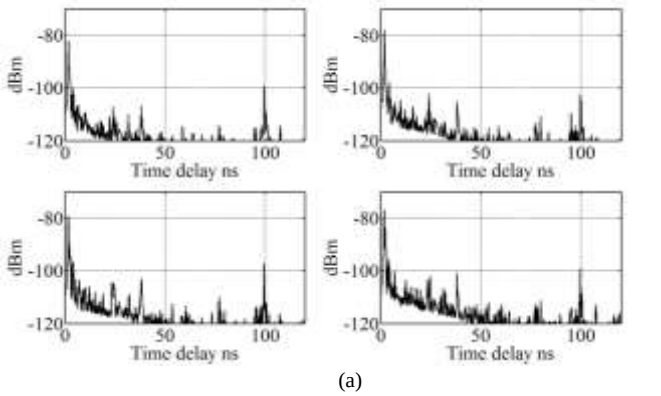

(a)

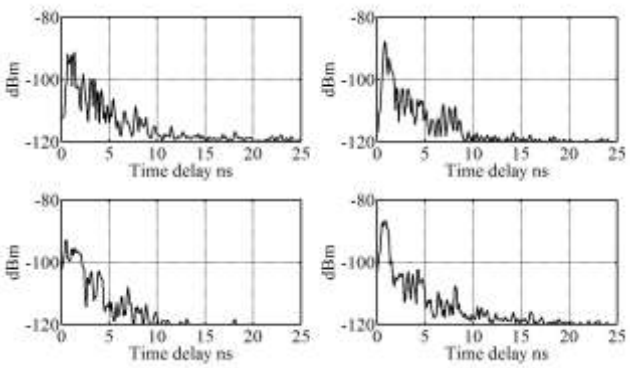

(b)

Fig. 9 PDP for the 2 by 2 MIMO channels (a) indoor, (b) outdoor

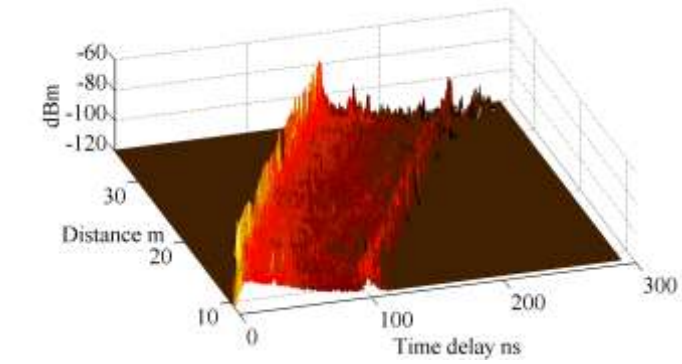

(a)

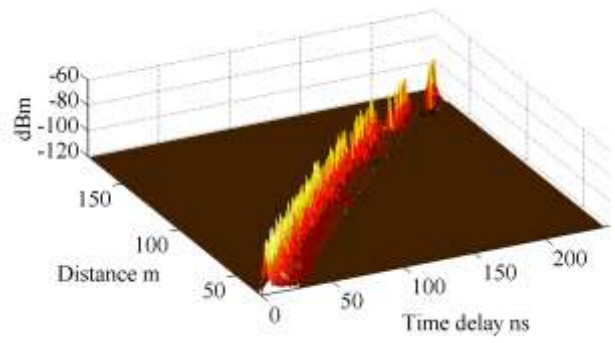

(b)

Fig. 10 PDP for single link as a function of distance (a) indoor, (b) outdoor

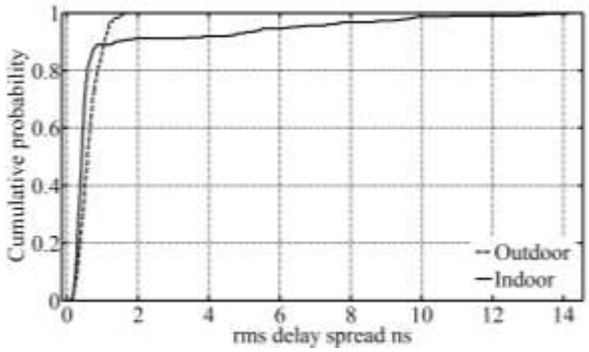

Fig. 11 CDF for rms delay spread for the indoor and outdoor environments

Table I

SUMMARY OF RMS DELAY SPREAD AND 20 DB WIDTH OF THE DELAY PROFILE FOR THE INDOOR AND OUTDOOR ENVIRONMENTS

% CDF	20 dB width ns		20 dB rms delay spread ns	
	indoor	outdoor	Indoor	outdoor
50%	3.3	4.5	0.4	0.6
90%	26.6	7.8	1.4	1
95%	99	8.3	6.3	1.2

that the rms delay spread values for both environments are comparable for 50% of the locations with an increase in delay spread in the indoor environment due to the glass façade which caused an increase in the delay spread for a number of the measured locations.

The path loss was also estimated for both environments using the least square algorithm which gave a path loss coefficient of ~1.6 for the indoor environment and ~1.9 for the outdoor environment shown in Fig.12. The indoor path loss coefficient is considerably smaller than the free space value of 2 which is typical of corridor indoor environments. Despite the presence of desks and chairs in the measured environment, it resembles a wide corridor with several reflective surfaces on either side.

The data were also analysed to estimate the MIMO capacity using the normalised complex frequency response $\boldsymbol{H}$ of the MIMO channel obtained over 1 second interval as in (7) and the results are displayed in Fig. 13 for both environments in comparison to the ideal independent and identically distributed (iid) channel and the theoretical single input single output capacity.

$$C = \frac{1}{N_f}\sum_{i=1}^{N_f} log_2\left[det\left(\boldsymbol{I}_{n_R} + \frac{\rho}{n_T}\boldsymbol{H}_i{\boldsymbol{H}_i}^H\right)\right] \quad (7)$$

where N_f is the number of frequency sub-channels; n_R and n_T are the number of receiver and transmitter antennas respectively; I_{nR} is the identity matrix; ρ is the SNR; *det(.)* is the matrix determinant; $\boldsymbol{H}_i$ is the $n_R x n_T$ normalised matrix containing the sample transfer function for sub-channel *"i"*; and $(.)^H$ is the matrix conjugate transpose.

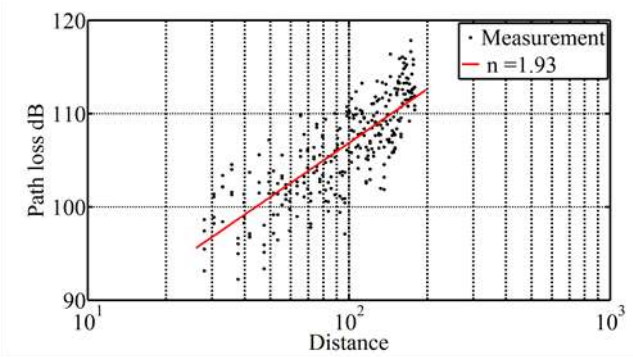

Fig. 12 Path loss fit for the outdoor environment

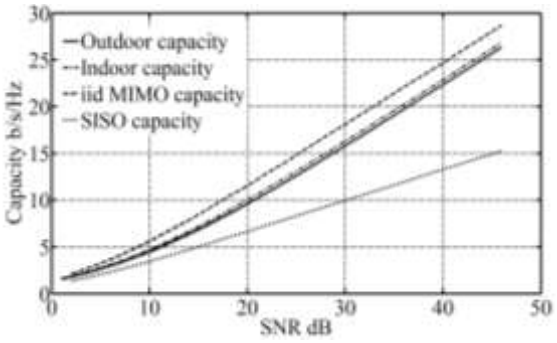

Fig. 13 Estimated MIMO capacity of the measured indoor and environment.

For each measurement snapshot the corresponding MIMO channel matrices are normalised using the Forbenious normalisation in (8) to provide an average unity gain.

$$\beta = \left(\frac{1}{N_f n_R n_T}\sum_{i=1}^{N_f}\sum_{k=1}^{n_R}\sum_{j=1}^{n_T}\left|H_{kj,i}\right|^2\right) \quad (8)$$

The data used in the estimation of the MIMO capacity were verified to have a SNR in excess of 25 dB for both environments. For 20 dB SNR, the results show that the MIMO capacity is 9.6 b/s/Hz, for the outdoor environment, and 10 b/s/Hz for the indoor environment which are fairly close to the ideal iid channel capacity of 11.6 b/s/Hz. The corresponding SISO capacity is 6.65 b/s/Hz.

In [16] the *rms* phase noise of the measurement system is shown to enhance the estimated MIMO capacity. The impact of phase noise on MIMO capacity was also studied in [4] and [17] from back to back measurements and in an anechoic environment. In [4] the *rms* value of phase noise was estimated to be 2^o within the measurement time and was considered appropriate for the estimation of MIMO capacity for different antenna configurations. Similarly the *rms* values of phase noise of the presented MIMO channel sounder were estimated in an anechoic environment since the two transmit and parallel receive configuration does not permit the simultaneous back to back measurement of all four transmit and receive combinations. The *rms* phase noise for the four MIMO channels was then estimated to be 2.3^o, 2.1^o, 2.3^o and 2.1^o which are close to the values observed in [4] and lower than the 3.5^o and 7^o values considered in [17]. In [4] the 2 by 2 MIMO capacity for a NLOS indoor environment was found to be close to the iid case with larger deviations observed as the SNR increased when the number of transmit and receive antennas increased from 2 by 2. Although in the measurements reported in this paper, the transmit and receive antennas were generally pointed toward each other, the enhanced MIMO capacity can be attributed to the multipath observed in both environments as seen from the *rms* values of delay spread and the width of power delay profile in Table 1.

IV. CONCLUSIONS

A wideband 2 by 2 MIMO channel sounder designed for the 60 GHz band was presented and its performance was demonstrated in terms of phase noise, dynamic range and isolation between the MIMO channels. The sounder was used for indoor and outdoor measurements to estimate channel parameters such as *rms* delay spread, path loss and MIMO capacity. Further enhancement of the sounder capability to the higher frequency bands up to 90 GHz is currently under development for 5G millimeter wave propagation studies. Using four units as shown in Fig.1, a multiple site hub will be set up to perform long term measurements to study the impact of rain on fixed point to point links for backhaul transmission.

REFERENCES

[1] S. Guillouard, G. El Zein and J. Citern, "Wideband propagation measurements and Doppler analysis for the 60 GHz indoor channel", *MTT IEEE- S digest*, pp. 1751–1754, 1999.

[2] C. R. Anderson, and T.S. Rappaport, "In-Building wideband partition loss measurements at 2.5 and 60 GHz", *IEEE Trans Wireless Communications*, vol. 3, no. 3, pp. 922–928, May. 2004.

[3] T. Zwick, T.J. Beukema, and H. Nam, "Wideband channel sounder with measurements and model for the 60 GHz indoor radio channel", *IEEE Trans. Veh. Technol.*, vol. 54, no. 4, pp. 1266–1277, Jul.2005.

[4] S. Ranvier, J. Kivinen, and P. Vainikainen, Millimeter-wave MIMO radio channel sounder, *IEEE Trans. on Instrum. and Meas.*, vol. 56, no. 3, pp. 1018–1024, Jun. 2007.

[5] M. Peter, W. Keusgen, "A Component-based time domain wideband channel sounder and measurement results for the 60 GHz in-cabin radio channel", *EUCAP 2007*, pp. 1–6, 2007.

[6] J. Kivinen, "60-GHz wideband radio channel sounder", *IEEE Trans. Instrum. Meas.*, vol. 56, no. 5, pp. 1831–1838, Oct. 2007.

[7] A.P.G. Ariza, R. Müller, F. Wollenschläger, A. Schulz, M. Elkhouly, Y. Sun, S. Glisic, U. Trautwein, R. Stephan, J. Müller, R.S. Thomä, and M.A. Hein, "60 GHz ultrawideband polarimetric MIMO sensing for wireless multi-gigabit and radar", *IEEE Trans. Antennas Propagat.*, vol. 61, no. 4, pp 1631–1641, Apr. 2013.

[8] P. F. M. Smulders and A. G. Wagemans, "Frequency-domain measurement of the millimeter wave indoor radio channel", *IEEE Trans. Instrum. Meas.*, vol. 44, no. 6, pp. 1017–1022, Dec. 1995.

[9] M. Kyrö, et.al, "Statistical channel models for 60 GHz radio propagation in hospital environments", *IEEE Trans. Antennas Propagt.*, vol. 60, no. 3, pp. 1569–1577, Mar. 2012.

[10] M. Kyrö, "Radio wave propagation and antennas for millimeter wave communications," Ph.D. dissertation, Dept. of Radio Science and Engineering, Aalto University, 2013.

[11] Y.I. Nechayev, X. Wu, C.C. Constantinou, P.S. Hall, "Effect of body motion on propagation path gain At 60 GHz", In Proc., *EUCAP 2012*, 2012, pp. 3397–3401.

[12] L. Talbi and J. LeBel, "Broadband 60 GHz sounder for propagation channel measurements over short/medium distances", *IEEE Trans. Instrum. Meas.*, vol. 63, no. 2, pp. 343–351, Feb. 2014.

[13] S. Feeney and S. Salous, “Implementation of a channel sounder for the 60 GHz band”, *In* Proc. URSI General Assembly, Chicago, 2008, pp. 1–4.

[14] S. Salous, *Radio propagation measurements and channel modelling*, Wiley, 2013.

[15] http://www.analog.com/media/en/technical-documentation/data-sheets/ADF4106.pdf

[16] D. S. Baum and H. Bolcskei, “Impact of phase noise on MIMO channel measurement accuracy”, *In* Proc. *VTC2004-Fall*. 2004 IEEE 60th, 2004, pp. 1614–1618.

[17] A. Taparugssanagorn and J. Ylitalo, “Characteristics of short-term phase noise of MIMO channel sounding and its effect on capacity estimation”, *IEEE Trans. on Instrum. and Meas.*, vol. 58, no. 1, pp. 196–201, Jan. 2009.